ligand displacement was used for the synthesis of bismuth β-diketonate complexes.

The most promising compound synthesized, in terms of precursors for MOCVD, was $Bi(fod)_3$. From these results, it appears that the reaction between 3 equiv of H(fod) and 1 equiv of triphenylbismuth produces the tris chelate. The mass spectral, NMR, GC/MS, and thermogravimetric analyses all indicate that the crude product appears to contain an extra fod ligand, perhaps existing as the tetrakis complex, $HBi(fod)_4$, or as an adduct with the fourth ligand only weakly associated. If the reaction product is carefully sublimed, however, the tris chelate is obtained. The following equilibrium may exist and be driven to the right as temperature is increased:

$$H[Bi(fod)_4] \text{ or } Bi(fod)_3 \cdot xH(fod) \overset{\Delta}{\rightleftharpoons} Bi(fod)_3 + xH(fod)$$

Elemental analysis of the residue remaining after sublimation or after use as a source for MOCVD indicates that some of the tris chelate decomposes to form a ligand-deficient nonvolatile species. Efforts were not made to remove the excess ligand from the chelate before using it as a MOCVD precursor, because the chelate was presublimed as part of the deposition experiment, and as has been noted previously,[17] the presence of excess ligand can improve the vaporization of the precursor compounds and is not detrimental to thin film formation. As postulated earlier for stabilization of Ba(II) complexes, the presence of excess ligand may also serve to repair ruptured chelate rings.[18]

In conclusion, the reactions of triphenylbismuth with several β-diketones have been investigated, and the reaction products have been characterized. The reaction with H(fod) to make $Bi(fod)_3$, perhaps via a tetrakis or ligand adduct intermediate species, was successful in producing a volatile chelate of bismuth that is a suitable precursor for making bismuth-containing thin films by MOCVD.

Acknowledgment. We thank Nancy Finnigan for performing the Auger analysis which was carried out in the Center for Microanalysis of Materials at the University of Illinois, which is supported by the US Department of Energy under Contract DE-AC 02-76ER 01198.

Registry No. $BiPh_3$, 603-33-8; $Bi(Fod)_3$, 141364-07-0; $Bi(hfa)_3$, 141364-06-9; Bi, 7440-69-9; $Bi(Fod)_2Ph$, 142188-44-1.

(17) Dickinson, P. H.; Geballe, T. H.; Sanjurjo, A.; Hildenbrand, D.; Craig, G.; Zisk, M.; Collman, J.; Banning, S.; Sievers, R. E. *J. Appl. Phys.* **1989**, *66*, 444.

(18) Turnipseed, S. B.; Barkley, R. M.; Sievers, R. E. *Inorg. Chem.* **1991**, *30*, 1164.

Bulk Semiconductors from Molecular Solids: A Mechanistic Investigation

W. E. Farneth,* N. Herron, and Y. Wang

Central Research and Development Department, The Du Pont Company, Wilmington, Delaware 19880-0356

Received December 12, 1991. Revised Manuscript Received April 27, 1992

We report on the mechanism of the solid-state conversion of a series of II/VI precursors of general formula $(R_4N^+)_4[S_4M_{10}(SPh)_{16}]^{4-}$ (R = Me, Et; M = Cd, Zn) to the bulk metal sulfide structure. On heating in vacuum or inert atmosphere, we find that the solid-state conversion proceeds in two discrete reaction steps. The first step, ~200 °C, can be characterized as a nucleophilic substitution or elimination initiated by the attack of a fragment of the anion cluster on the tetraalkylammonium counterion. The intermediate solid produced in this step consists of charge neutral $M_{10}S_{16}Ph_{12}$ clusters that retain the primary cluster size present in the starting material but appear to aggregate to varying degrees in the solid or solution. The intermediate cluster has very different chemical and physical properties from the starting material and, therefore, suggests some new possible routes to the preparation of bulk II/VI semiconductor films and powders from molecular precursors.

Introduction

The preparation of crystalline solids via the consolidation of molecular precursors is an increasingly important branch of solid-state chemistry.[1] II/VI compound semiconductors have been a favorite subject for such studies because of interest in the evolution of their electronic properties as the consolidation process proceeds. Consequently, a wide variety of molecular precursor approaches to these materials has been described.[2,3] Nevertheless, whether the goal is crystalline thin films via MOCVD or microcrystalline powders via solution- or solid-state reactions, detailed information on the mechanisms of the transformation from molecules to bulk II/VI solids is limited. In this paper we report on the mechanism of the solid-state conversion of a particular series of II/VI precursors of general formula $(R_4N^+)_4[S_4M_{10}(SPh)_{16}]^{4-}$ to the bulk metal sulfide structure. On heating, in vacuum or

(1) Rao, C. N. R.; Gopalakrishnan, J. *New Directions in Solid State Chemistry*; Cambridge University Press: Cambridge, UK 1986; Chapter 3. (b) Spanhel, L.; Anderson, M. *J. Am. Chem. Soc.*, **1990**, *113*, 2826 and references therein.

(2) (a) Brennan, J. G.; Siegrist, T.; Carroll, P. J.; Stuczynski, S. M.; Reynders, P.; Brus, L. E.; Steigerwald, M. L. *Chem. Mater.* **1990**, *2*, 403 and references therein. (b) Bawendi, M. G.; Kortan, A. R.; Steigerwald, M. L.; Brus, L. E. *J. Chem. Phys.* **1989**, *91*, 7282.

(3) Osakada, K.; Yamamoto, T. *J. Chem. Soc., Chem. Commun.* **1987**, 1117. Osakada, K.; Yamamoto, T. *Inorg. Chem.* **1991**, *30*, 2328.

0897-4756/92/2804-0916$03.00/0

inert atmosphere, we find that the solid-state conversion proceeds in two discrete reaction steps. The first can be characterized as a reaction (nucleophilic substitution or elimination) of a fragment of the anion cluster with the tetraalkylammonium counterion. As a result, the intermediate solid consists of charge neutral clusters of overall stoichiometry $M_{10}S_{16}Ph_{12}$ which are highly soluble in pyridine. Further heating then cleanly converts this molecular intermediate to the extended metal–sulfide lattice at temperatures below 550 °C.

Experimental Section

X-ray powder diffraction measurements were performed with a Scintag automated powder diffractometer using Cu Kα radiation. Electronic spectra were recorded in 1-mm-path-length quartz cells using a Perkin-Elmer 559 UV–vis spectrophotometer. Photoluminescence spectra were taken on a Spex Fluorolog fluorimeter, all of the reported spectra being corrected for the photomultiplier response. Samples were cooled in a continous-flow helium cryostat (Oxford Instruments CF1204). Thermogravimetric analyses were performed either in flowing nitrogen (100 cm^3/min) or vacuum using a Du Pont Instruments 950 TGA. TGA/mass spectral studies were carried out using a modified Cahn RG microbalance enclosed in a high-vacuum chamber. The evolved gas stream from the microbalance chamber was monitored with a UTI quadrupole residual gas analyzer.[4] All synthetic procedures and sample manipulations were carried out in an inert-atmosphere (nitrogen) drybox from Vacuum Atmospheres (<10 ppm oxygen, <10 ppm water). Solvents for synthesis and optical measurements were dried and deoxygenated by standard techniques. ^{113}Cd NMR spectra were collected on spinning and proton-decoupled solutions of the cadmium compounds in 10-mm tubes using a GE instruments 300-MHz spectrometer operating at 66.655 MHz. Shifts are referenced to 0.1 M cadmium nitrate in water ($\delta = 0$). 10% deuterium was incorporated into the solvent for purposes of frequency locking. FT Raman spectra were recorded on a Nicolet 800 interferometer equipped with a CaF_2 beam splitter and a Ge detector operated at 77 K. The spectral resolution was 2 cm^{-1}, and an LDP2000 diode pumped Nd:YAG laser was used as the excitation source. The power levels were maintained between 50 and 100 mW. All spectra were referenced to a white light spectrum to correct for instrument response. Frequencies were accurate to ±2 cm^{-1}.

The compounds $(NR_4)_4(S_4M_{10}(SPh)_{16})$ (I, where R = Me, and M = Cd, Zn) were prepared in the glovebox following the published procedures[5] and were recrystallized from acetonitrile as large colorless blocks or needles, respectively. X-ray powder diffraction (Figure 1) patterns for the Cd materials confirm the nature of the materials. The new compound, where R = Et and M = Cd, was prepared as follows, using a modification of the published procedure substituting tetraethylammonium chloride directly in place of the reported tetramethyl reagent. All chemical analyses were carried out by Galbraith Labs, Knoxville, TN.

$(Et_4N)_2[Cd_4(SPh)_{10}]$. A solution of $Cd(NO_3)_2{\cdot}4H_2O$ (21 g) in 60 mL of methanol was quickly added to a stirred solution of 20 g of thiophenol and 18.5 g of triethylamine in 60 mL of methanol at room temperature in an inert atmosphere glovebox. When thoroughly mixed, a solution of 12.7 g of tetraethylammonium chloride in 40 mL of methanol was added all at once. After brief stirring, the solution became clear and was left undisturbed at 0 °C while a viscous oily layer separated in the bottom of the flask. The top layer of methanol was decanted, and the oily layer was washed and triturated with more methanol, whereupon it solidified to a low melting point white solid; 20.4 g of solid was recovered for a yield of 66%. This solid was used directly in the following procedure.

$(Et_4N)_4[S_4Cd_{10}(SPh)_{16}]$. Sulfur powder (0.3 g) was added to a stirred solution of 16 g of $(Et_4N)_2[Cd_4(SPh)_{10}]$ in 50 mL of acetonitrile at room temperature in an inert-atmosphere glovebox.

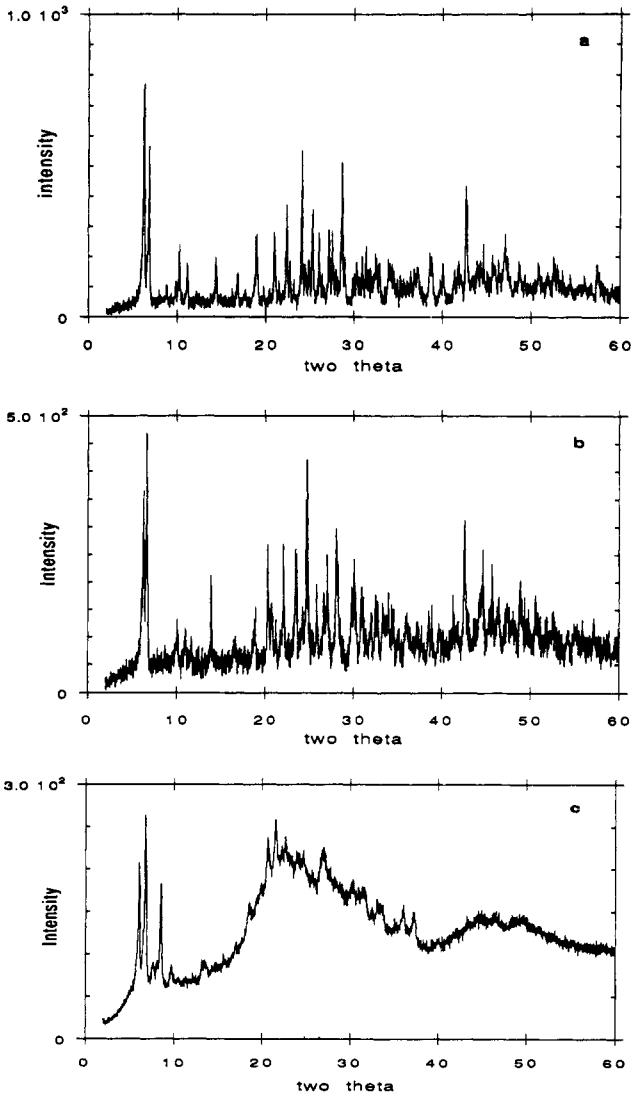

Figure 1. Collage of X-ray powder diffraction patterns for key materials: (a) $(R_4N^+)_4[S_4M_{10}(SPh)_{16}]^{4-}$ (R = Me, M = Cd) (I), (b) same as (a) (R = Et), (c) intermediate II obtained from thermolysis of I, recrystallized from pyridine.

After 30 min of stirring, the sulfur had dissolved and the solution was cloudy with a white precipitate. Acetonitrile (150 mL) was added, and the solution was heated close to the boiling point of acetonitrile in order to dissolve the precipitate and generate a clear solution. Upon cooling overnight, large colorless laths of the desired compound were deposited from the acetonitrile and were collected by filtration to yield 5.1 g, 65%. Their identity was confirmed by the similarity of the powder X-ray diffraction pattern to that of the well-characterized NMe_4 analogue (see Figure 1b). Anal. Calcd: 43.68% C; 4.58% H; 1.59% N; 18.22% S; 31.93% Cd. Found: 43.49% C; 4.28% H; 1.69% N; 18.25% S; 31.74% Cd.

Bulk samples of the intermediate $M_{10}S_{16}Ph_{12}$, identified from the TGA experiments (vide infra), were prepared by heating I in quartz tubes attached to a high-vacuum line. Samples of I (500 mg) were heated at 10 °C/min to 300 °C and held there for 15 min, all in dynamic vacuum. The orginally white/colorless crystals become pale yellow in the case where M = Cd but remain white where M = Zn. Anal. Calcd: 33.75% C; 2.36% H; 0.0% N; 20.02% S; 43.87% Cd. Found: 34.05% C; 2.47% H; <0.50 % N; 20.35% S; 43.46% Cd. Despite the fact that the well-formed crystals of I maintain their shape during this procedure, they are no longer single crystals and display powder X-ray diffraction patterns typical of extremely small, sphalerite-structure particles of <10 Å diameter (vide infra). These materials are completely soluble in dry pyridine but insoluble in DMF, in complete reversal of the solubility of their precursors I. Pyridine solutions may be induced to produce small, well-formed, colorless cyrstals (together

(4) Farneth, W. E.; Ohuchi, F.; Staley, R. H.; Chowdhry, U.; Sleight, A. W. *J. Phys. Chem.* **1985**, *89*, 2493.
(5) Dance, I. G.; Choy, A.; Scudder, M. L. *J. Am. Chem. Soc.* **1984**, *106*, 6285.

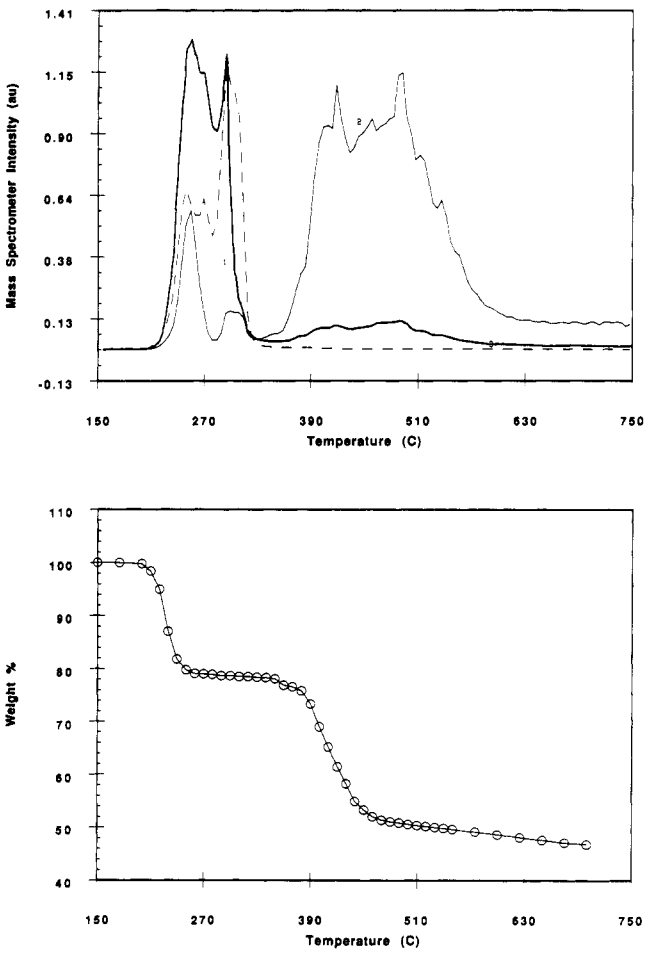

Figure 2. (a) Mass spectral intensity profiles for m/e 58 (curve 1, solid), m/e 110 (curve 2, solid), and m/e 124 (curve 3, dashed) in vapor evolved from (I) during 10 °C/min ramp in vacuum. Intensity data are uncorrected for detector response or fragmentation from higher mass ions and therefore do not represent absolute partial pressures of individual components of the vapor stream. The temperature range of the mass spectral features is broadened relative to the corresponding mass changes shown in (b) due to mass transport effects. (b) Weight loss of I in vacuum during 10 °C/min ramp.

with a yellow/cream powder) by slow vapor in-diffusion of methanol over a period of several days, and such crystals give rise to the powder diffraction pattern shown in Figure 1c.

Results

(1) TGA of I. *(a) R = Me; M = Cd.* The chemistry that occurs as the molecular cluster $[(CH_3)_4N^+]_4[S_4Cd_{10}(SPh)_{16}]^{4-}$ is heated in an inert atmosphere has been followed by combined TGA and mass spectroscopy as shown in Figure 2. Both mass loss of the solid and mass spectroscopy of the evolved gas show two well-resolved features corresponding to two different reaction events occurring between 100 and 500 °C. The first reaction, giving the TGA/ms feature centered around 200 °C, corresponds very well with loss of mass equivalent to $4(NMe_4SPh)$. The loss of the cluster countercations implied by this weight change produces a new molecular solid of stoichiometry $Cd_{10}S_{16}Ph_{12}$ which we have isolated and recrystallized. This intermediate structure will then undergo a second reaction, beginning around 350 °C (Figure 2). Mass loss is equivalent to S_6Ph_{12}, leaving a solid residue with the stoichiometry CdS. Anal. Calcd: 0.0% C; 22.19% S; 77.81% Cd; 0.0% H; 0.0% N. Found: 1.09% C; 21.82% S; 76.75‰ Cd; <0.5% H; <0.5% N). X-ray diffraction demonstrates that this solid is essentially phase-pure CdS

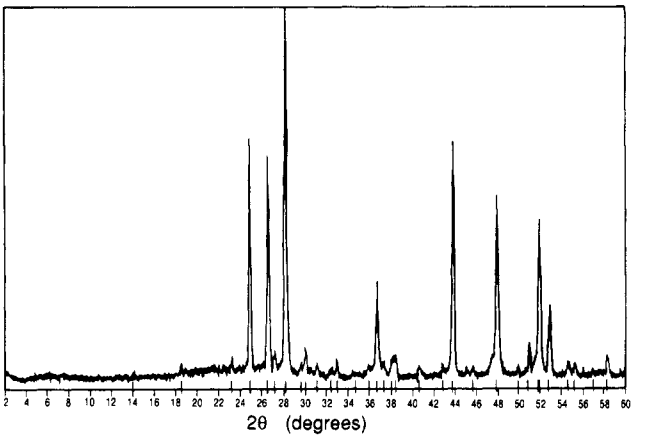

Figure 3. X-ray powder diffraction of CdS obtained from thermolysis of I.

in the Wurtzite structure. The diffraction data suggest that the cluster size of the CdS obtained from this treatment is considerably larger than the starting cluster I (~30 vs 7 Å) but still consists of very small crystallites. However, cluster size may be sensitive to the specific conditions under which the solid-state reactions are carried out, and we have done nothing to optimize either the size or size distribution in the product. Further heating, to temperatures beyond the range of these TGA experiments (700–900 °C) converts the material to the macrocrystalline, bulk wurtzite phase (Figure 3).

The gas-phase products formed in the two weight-loss events shown in Figure 2 are quite different. Mass spectroscopy indicates that the two principal products of the low-temperature event are trimethylamine, $N(CH_3)_3$ [m/e = 58, 43, 28] and methyl phenyl sulfide, CH_3SPh [m/e = 124, 123]. A small amount of thiophenol, HSPh [m/e = 110, 66, 109] is also observed. The onset temperature for the m/e 58 and 124 ions is identical, and they both grow rapidly with similar intensity profiles as the temperature is raised. This suggests that their evolution into the vapor phase is controlled by the same rate constant, which is most likely the chemical reaction rate constant for their simultaneous formation. The mass spectral profiles for all of the key ions are double peaked, which may indicate that there are two stages to this reaction that are not separately resolved in the TGA experiment.

The chemistry of the second event (350–450 °C) is apparently a little more complex. The temperature range over which this reaction occurs is somewhat wider and tails out to higher temperature. In the mass spectral profiles, diphenyl sulfide [m/e = 186, 185] thiophenol, biphenyl [m/e = 154, 153], and perhaps smaller amounts of other products are observed. In Figure 2 the m/e = 110 trace is shown to represent the temperature profile of the second event. At the high-temperature end, the small, continuing weight-loss seems to produce mostly H_2S in the vapor phase. The two plateau regions in the TGA correspond very well with the residual stoichiometries, $Cd_{10}S_{16}Ph_{12}$ (expected weight = 77.8%) for the first-formed intermediate, and $Cd_{10}S_{10}$ (expected weight = 44.0%) for the ultimate product. This implies that both reactions proceed to completion to form homogeneous solid substances.

(b) R = Me, M = Zn. The same decomposition sequence is observed for the Zn analogue of I (Figure 4). The major differences between the Zn and Cd compounds are a slight shift to higher temperature for the first event, a wider temperature range for the second event, and the possible resolution of two steps in the second feature. The higher temperature required to remove the caps from the ZnS

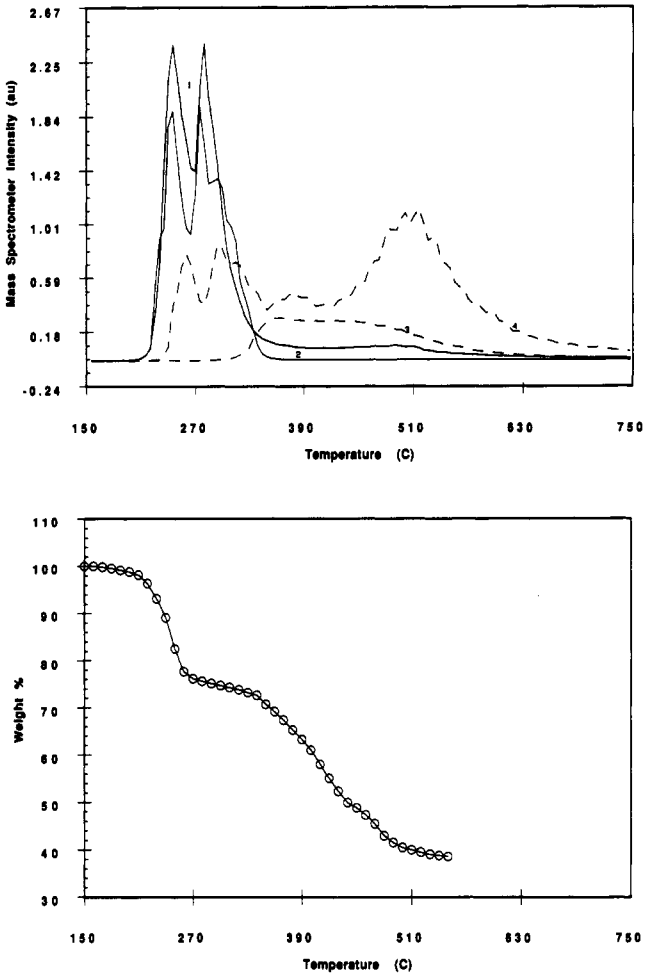

Figure 4. As in Figure 2. Starting material is I; M = Zn. (a) m/e 58 (curve 1, solid), m/e 124 (curve 2, solid), m/e 186 (curve 3, dashed), m/e 110 (curve 4, dashed). (b) Expected residual weight for $Zn_{10}S_{16}Ph_{12}$ = 74.0%; expected residual weight for $Zn_{10}S_{10}$ = 34.5%.

cluster is consistent with the observations of Steigerwald et al. on the formation of II/VI materials from M(SePh)$_2$(DEPE) clusters.[2] Loss of volatile molecules associated with the second reaction (PhSPh, HSPh) appears to begin almost as soon as the first event is completed, implying that the molecular intermediate has a narrower stability range in the Zn system.

2. Structure of I: Uniqueness of Tetrahedral Corners. The crystal structure of I is shown in Figure 5.[5] There are four unique SPh^- ligands associated with the corners of the tetrahedral cluster. From the stoichiometry of products during the thermal transformation described above, it appears that a useful way to think about the first step in the solid-state transformation of this material to bulk semiconductor is that reaction occurs specifically at the tetrahedral corners. The reaction mechanism may then involve a nucleophilic attack of the unique SPh^- that caps the corner Cd atoms on a methyl group of the proximal Me_4N^+. To test this model, we have prepared the tetraethylammonium cation of I, R = Et, M = Cd. In this material, nucleophilic attack by SPh^- could lead to either a substitution reaction, the analog of the chemistry observed with Me_4N^+, producing EtSPh + Et_3N or, since there are now available β-hydrogen atoms on the cation, an elimination reaction producing HSPh + C_2H_4 + Et_3N.

Figure 6 shows the TGA/ms data for the Et_4N^+ compound. Weight loss begins at about 175 °C, about 50 °C lower than in the Me_4N^+ material, and there are clearly

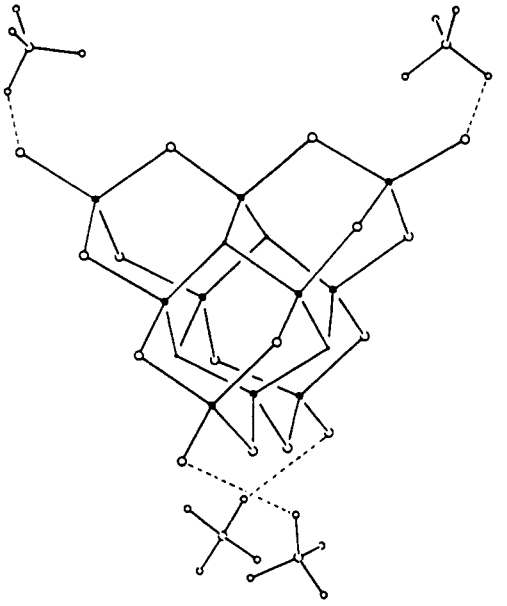

Figure 5. Schematic diagram of the crystal structure of I, ● = Cd. Two types of S are distinguished: · = S triply coordinated to Cd, O = bridging or terminal SPh. The tetramethylammonium cations are shown in association with their nearest neighbor S: o = CH_3, O = N. Phenyl substutents and H atoms have been omitted for clarity.

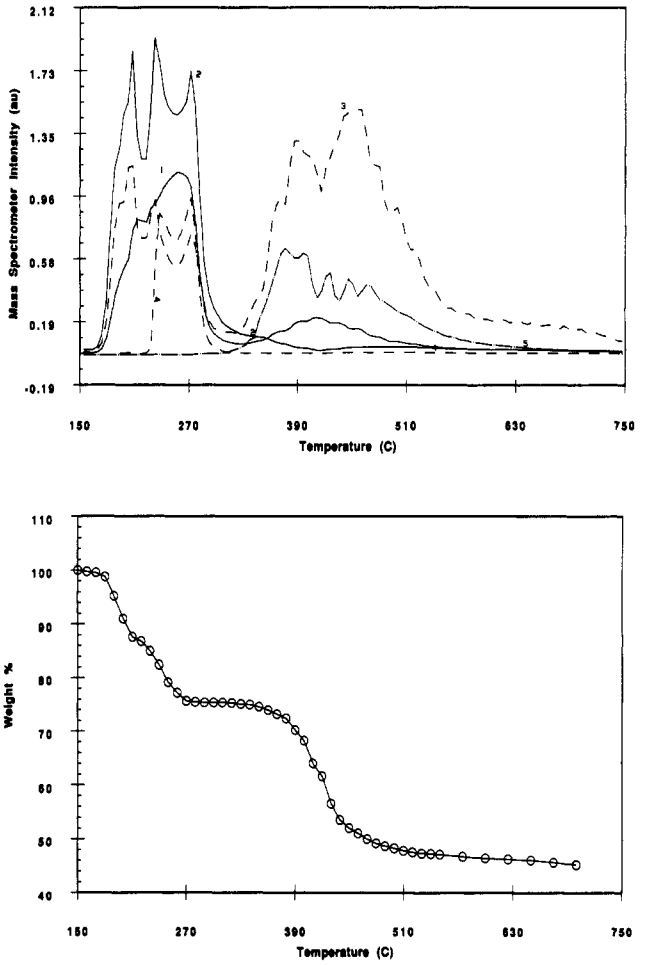

Figure 6. As in Figure 2. Starting material is $(Et_4N)^+$ salt of I. (a) m/e 27 (curve 1, solid), m/e 86 (curve 2, solid), m/e 110 (curve 3, dashed), m/e 138 (curve 4, dashed), m/e 186 (curve 5, dash-dot).

two stages to the low-temperature weight-loss event. The first stage of the reaction produces the elimination prod-

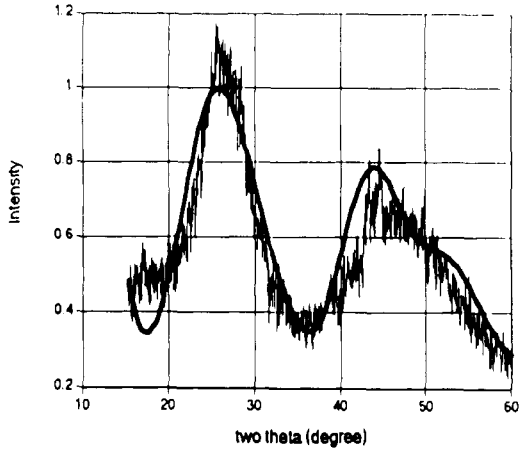

Figure 7. X-ray powder diffraction pattern of intermediate II. The solid line is a fit to the experimental data based on the atomic positions in the crystal structure of the starting material I.

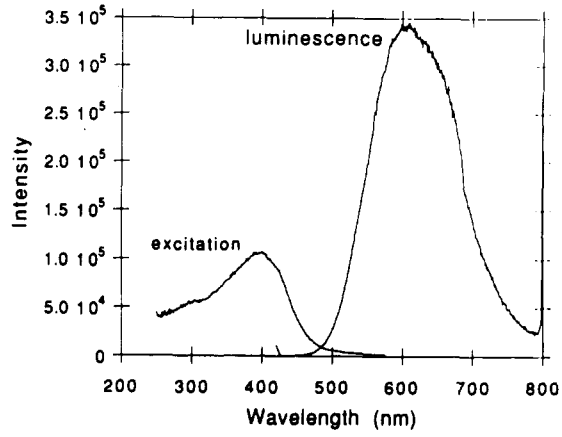

Figure 8. Excitation and luminescence spectra of a polycrystalline powder of the intermediate II obtained from the solid-state thermolysis of I.

ucts HSPh, C_2H_4, and Et_3N. The onset temperature for the substitution chemistry is signalled by the appearance of EtSPh in the mass spectral profiles at about 225 °C, the same as the onset temperature for decomposition of the Me_4N^+ material. The stable intermediate stoichiometry, $Cd_{10}S_{16}Ph_{12}$, is the same as that obtained in Figure 2 from Me_4N^+, and it is reached at essentially the same temperature. The TGA/ms of the second weight-loss event is indistinguishable from the Me_4N^+ compound.

(3). Characterization of the Intermediate $Cd_{10}S_{16}Ph_{12}$. We have isolated and characterized the intermediate $Cd_{10}S_{16}Ph_{12}$ material (II). We have studied the properties of II under three types of conditions: as powders produced from the solid-state thermolysis of I, in pyridine solution, and as a recrystallized solid.

Raman spectra (200–3300 cm^{-1}) of the powders show distinct differences between the starting materials (I) and the intermediate (II) in both the high- and low-frequency regimes. Aliphatic C–H stretches beween 2900 and 3000 cm^{-1} are present in the starting solid but are not present in the intermediate. Aromatic C–H stretches around 3050 cm^{-1} are present in the intermediate, but with a somewhat broader frequency distribution. On the low-frequency end, the strong Raman line at 240 cm^{-1} which Dance et al.[5] suggested may be associated with Cd–S vibrations of bridging thiolate species has disappeared in the intermediate. If this is the correct assignment, it would be inconsistent with a reaction that had specifically removed the terminal thiolate ligands as we have suggested. We are continuing work in this area with structural analogues, wider frequency ranges, and IR spectroscopy to obtain a clearer picture of the changes in bonding accompanying this structural change.

Solution-phase ^{113}Cd NMR of II in pyridine shows two peaks at δ = 630 and 422.5 ppm in a ratio of 3:2. Although this is the intensity ratio that would be expected from an intermediate that has retained the basic tetrahedral cluster geometry of I, the high-field resonance is very broad and shows evidence of becoming resolved into three peaks of equal intensity. It seems likely that Cd sites are in dynamic equilibrium on the NMR time scale under these conditions as has been observed in other Cd–S cluster compounds.[6] Low- (–20 °C) and high- (80 °C) temperature NMR, however, fails to sharpen these resonances significantly. ^1H NMR at room temperature in pyridine-d_5 shows only the expected doublet (δ = 7.9 ppm) and a pair of triplets (δ = 7.0, 6.9 ppm) of the 12 equivalenced capping thiophenol groups.

The X-ray powder diffraction pattern of the material produced by heating to 300 °C as described above, is shown in Figure 7. The pattern shows two peaks at 2θ = 26° and 2θ = 45° with a prominent shoulder at 53°. As shown in the figure, this pattern can be successfully simulated using known positions of Cd and S atoms within the individual tetrahedral clusters of I, M = Cd. The simulation is obtained by calculation of a diffraction pattern of the sphalerite core of I. The peak at 2θ of 26° corresponds to the (111) peak of bulk CdS, at 2θ of 25.9°. Previously we have shown that this (111) peak moves to 28.5° when a similar cluster containing a sphalerite core, grows to >10-Å size.[8] The agreement in both peak width and peak position shown in Figure 7 therefore suggests that the individual clusters retain their integrity in the transformed solid and that there are not large changes in the local structures of the Cd–S core of the clusters as a result of this transformation. The three-dimensional crystalline packing of these tetrahedral clusters in I is obviously lost during the thermal conversion process, however (compare Figure 1a).

Although the structural integrity of the clusters appears to be maintained in the solid, new electronic interactions between the clusters do exist as revealed by their optical properties. Figure 8 shows the luminescence and excitation spectra of powders of II. The luminescence spectrum is red-shifted from the absorption spectrum, which is typical of CdS clusters. The excitation spectrum reveals that the intermediate solid has an absorption band at 400 nm. This cannot be attributed to isolated $Cd_{10}S_{16}Ph_{12}$ clusters, since such small clusters would be expected to show only absorption in the 290–300-nm region.[7,8] The 400-nm band is due to either aggregates of $Cd_{10}S_{16}Ph_{12}$ or larger CdS clusters. We favor the former explanation since the latter possibility is not consistent with the X-ray results.

The optical properties of $Cd_{10}S_{16}Ph_{12}$ in pyridine solution are different from those in the solid state. Figure 9 shows the absorption, luminescence, and excitation spectra. The major absorption peak is located at ~300 nm, the same as that of the 7-Å starting cluster, $(Cd_{10}S_4(SPh)_{16})^{4-}$. Note that previously we have shown the absorption peak of a 10-Å $(Cd_{20}S_{13}(SPh)_{22})^{-8}$ cluster shifts to 350 nm[7] in

(6) (a) Haberkorn, R. A.; Que, L.; Gillum, W. O.; Holm, R. H.; Liu, C. S.; Lord, R. C. *Inorg. Chem.* **1976**, *15*, 2408. (b) Dance, I. G. *Aust. J. Chem.* **1985**, *38*, 1745.

(7) Herron, N.; Wang, Y.; Suna, A. *J. Chem. Soc., Dalton Trans.*, in press.

(8) Wang, Y.; Herron, N. *J. Phys. Chem.* **1991**, *95*, 525.

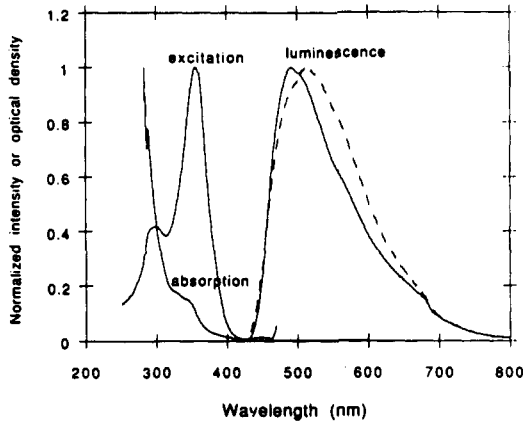

Figure 9. Absorption, excitation, and luminescence spectra of II in pyridine solution.

pyridine solution. The optical absorption data in solution are therefore consistent with the X-ray data, both indicating the size of the primary cluster is <10 Å.

In the absorption and excitation spectra, there is also a weaker absorption peak at ~346 nm. The intensity of this absorption decreases sublinearly with decreasing $Cd_{10}S_{16}Ph_{12}$ concentration. This result eliminates the possibility that this absorption is due to Cd–pyridine transition of an isolated cluster. Instead, we attribute it to the absorption of small aggregates of $Cd_{10}S_{16}Ph_{12}$ clusters. Apparently, there is a driving force for cluster–cluster aggregation in both solution and solid state. The aggregation we refer to involves chemical interaction between the clusters. In the Discussion, we will discuss the possible nature of these aggregates.

The solid can be recrystallized from pyridine solution by slow diffusion of alcohol, ether, or DMF. The recrystallized material has the crystalline diffraction pattern shown in Figure 1c and displays similar luminescence and excitation spectra to the solid-state reaction product. This implies that aggregates similar to those formed during the thermal synthesis are also obtained during recrystallization. Attempts to collect single-crystal X-ray diffraction data on these crystals are in progress, the colorless blocks of material being severely twinned. TGA shows that pyridine is present in the recrystallized solid at a stoichiometry of approximately 2 pyridine/cluster. The pyridine molecules, however, are weakly held and desorb intact at about 100 °C. The pyridine is presumably coordinated at remaining vacant Cd coordination sites on the cluster and does not significantly perturb the electronic structure.

Discussion

This work demonstrates that a stable intermediate, $Cd_{10}S_{16}Ph_{12}$, can be produced by thermally removing four terminal thiophenolate groups from $(Cd_{10}S_4(SPh)_{16})^{4-}$. This is surprising, since the removal of four terminal thiophenolate groups leaves four terminal Cd atoms uncoordinated. We expect that these exposed Cd atoms have to be either "capped" by coordination with other atoms or some kind of rehybridization has to occur. Rehybridization usually involves large changes in the structure and electronic properties, which is not implied by either the X-ray or the optical data. We therefore believe capping of the terminal Cd atoms occurs.

A careful examination of the structure of $(Cd_{10}S_4(SPh)_{16})^{4-}$ reveals that if the structural integrity of the cluster is to be maintained in the intermediate (II), there are two ways for the additional Cd coordination to occur. The terminal Cd atoms can coordinate to the terminal Cd atoms of other clusters, forming a Cd(III)–Cd(I) bond, or they can coordinate to the tricoordinate sulfur atoms on the facets of the pyramid (either inter- or intramolecularly), forming a tetrahedral sulfur bonded to four cadmium atoms. The latter possibility seems more attractive to us since it can explain the long-wavelength absorption observed in the excitation spectra of II. It is known that the lowest optical absorption of either bulk CdS or CdS clusters corresponds mostly to the transfer of an electron from a tetrahedral sulfur (HOMO or valence band) to cadmium atoms (LUMO or conduction band).[6] In either the $(Cd_{10}S_4(SPh)_{16})^{4-}$ or the $Cd_{10}S_{12}Ph_{16}$ clusters, there is no tetrahedral sulfur and the optical absorption bands of isolated clusters with these stoichiometries correspond to that of the Cd–thiophenolate moiety. Previously, we have shown that when a tetrahedral sulfur is formed within isolated clusters by increasing the cluster size from 7 to 10 Å, a sharp absorption band appears at 350 nm, corresponding to the sulfur to cadmium HOMO–LUMO transition.[7] The same tetrahedral sulfur coordination geometry can be formed in the solid state of II by coordinating the terminal Cd atoms of one cluster to the trivalent sulfur atoms of another cluster. The presence of such tetrahedral sulfur atoms could explain the long-wavelength absorption band observed for cluster aggregates.

In pyridine solution, solvent can coordinate to the terminal Cd atoms of $Cd_{10}S_{16}Ph_{12}$ and break up the aggregates. The solution absorption spectrum, with principal absorption below 300 nm, is essentially similar to that of $(Cd_{10}S_4(SPh)_{16})^{4-}$. This suggests isolated $Cd_{10}S_{16}Ph_{12}$ clusters. However, even in pyridine some aggregation still occurs as revealed by the presence of a weak absorption band at 346 nm. The location of this band is almost the same as that of the 10-Å $(Cd_{20}S_{13}(SPh)_{22})^{-8}$ cluster, which contains only one tetrahedral sulfur atom. It is tempting to attribute this band to the dimer of $Cd_{10}S_{16}Ph_{12}$, which also contains only one tetrahedral sulfur atom.

There are two generalizations which we think are useful implications of this work. The first is the demonstration that a solid-state chemical reaction can be a preparative route to new molecular cluster solids. There are few well-characterized molecular semiconductor clusters and the rational design of molecular precursors is an aspect of inorganic synthesis that is still in its infancy. Here is a new route to consider which, at least for these clusters derived from a tetrahedral segment of the sphalerite metal chalcogenide lattice, does not depend on the specific metal or alkyl ammonium ion that is present. In this case the new molecular cluster has quite different chemical and physical properties from the starting material. One of the technological advantages that these surface passivated molecular clusters promise is their processability. They can be thought of, for example, as soluble reagents that are precursors to semiconductor films. Therefore, the manipulation of their solubility and ionic charge can also be an important element in optimizing their utility. We have already demonstrated, for example, the possibility of spray depositing films of both CdS and the $Cd_{10}S_{16}Ph_{12}$ intermediate onto quartz, sapphire and KBr substrates.[9]

The second is the implication that ligand chemistry might be used to control the microstructural evolution during the transformation from molecular to extended solids. One of the key problems in taking advantage of the unique optical and electronic properties of nanometer-sized semiconductor clusters is the development of methods that permit mono-sized clusters to be prepared. In contrast to solution preparation methods, solid-state

(9) G. Blanchet, unpublished work.

reactions of molecular precursors offer the advantage of a cluster size distribution that is controlled by the reactant structure rather than the kinetics of the cluster formation reaction. Of course, in the case we have investigated, the homogeneous cluster size of the starting material appears to be lost during the transition from the intermediate to the extended solid. Nevertheless, the controlled chemistry that occurs during the first step suggests a number of possible ways to use ligand reactivity to influence the course of the solid-state reactions.

Acknowledgment. We are grateful to Bruce Chase for help with the collection and interpretation of Raman data, Fred Davidson for similar assistance with Cd NMR, Graciela Blanchet for preliminary spray deposition of thin films, and Cathy Foris for powder X-ray data. Jack Jensen, Sarah Harvey, and Willis Dolinger provided excellent technical help.

Main Effects in the Syntheses of Cu/Cr Layered Double Hydroxides

Robert P. Grosso, Jr.,[†] Steven L. Suib,*[,†,‡] Robert S. Weber,[§] and Paul F. Schubert[⊥]

Department of Chemistry and Institute of Materials Science, U-60, University of Connecticut, Storrs, Connecticut 06269-3060; Department of Chemical Engineering, University of Connecticut, Storrs, Connecticut 06269-3060; Department of Chemical Engineering, Yale University, New Haven, Connecticut 06520; and Catalytica, Mountain View, California 94043

Received January 24, 1992. Revised Manuscript Received June 3, 1992

Introduction

Layered double hydroxides (LDHs) are layered materials with anion-exchange properties. These materials are based on the layered mineral brucite, which consists of hydroxyl layers surrounding Mg^{2+} ions in an octahedral coordination.

The formula of LDHs can be written as follows:

$$M_x^{2+}M_y^{3+}(OH)_{2x+2y}A_{y/n}^{n-}\cdot zH_2O$$

Divalent and trivalent cations are bound in edge-shared octahedra of hydroxyl ions. Anions (A^{n-}) can be intercalated, and water molecules are loosely bound between hydroxyl layers.

Considerable recent interest in LDHs is most likely due to their numerous uses. LDHs have been used as selective heterogeneous catalysts and, surprisingly, are quite thermally stable. Some of the pillared phases used for catalysis are stable over 500 °C.[1] LDHs containing halide ions have shown promise in converting alkyl bromides to the respective alkyl halides.[2] Alkyl halide products were normally obtained with 80% yields at temperatures of 150 °C. Larger (100%) yields could be attained if excess LDH was used. A variety of different cations and anions have been used to prepare transition-metal LDHs.[3] Anions recently used to pillar LDHs include the ruthenium tris(4,7-diphenyl-1,10-phenanthrolinedisulfonate) anion ($Ru(BPS)_3^{4-}$), the first transition-metal luminescent complex to be incorporated into an LDH host,[4] and the anionic dyes indigo carmine and new coccine.[5]

Anions incorporated between the octahedral layers in LDHs are mobile. This anionic mobility has led to research on these materials as ionic conductors. Ionic conductivities of 10^{-3} and 10^{-4} Ω^{-1} cm^{-1} have been reported.[6] Anion mobility is unusually high due to swelling of the layers by a considerable H_2O sorption. Halides, nitrates, and carbonates have been studied. Proton-hopping mechanisms have also been reported. Proton hopping in LDHs occurs via H_2O molecules in the anionic layers.[7,8]

LDHs are good anion exchangers due to the mobility of anions. The anion exchange capacity of LDHs allows preparation of new LDH materials containing anions that do not incorporate by direct crystallization from aqueous solution. The anions Cl^-, ClO_4^-, and SO_4^{2-} have been incorporated in LDHs via anion exchange of hydrotalcite.[9] Miyata has used naphthol yellow S, an anionic dye, to study anion-exchange capacities of LDH or hydrotalcite-like compounds.[10] Other anions that have been exchanged into LDHs include silicate anions[11] and short- and long-chain organic anions.[12] Drezdzon has exchanged isopolymetalate ions, $Mo_7O_{24}^{6-}$ and $V_{10}O_{28}^{6-}$, into hydrotalcite.[13] In this technique, a hydrotalcite containing terephthalate (TA) is used as a precursor and is synthesized prior to the anion-exchange step. Once the Mg_4Al_2-

[†] Department of Chemistry and Institute of Materials Science, University of Connecticut.
[‡] Department of Chemical Engineering, University of Connecticut.
* To whom correspondence should be addressed.
[§] Yale University.
[⊥] Catalytica.

(1) Pinnavaia, T. J. *Science* **1983**, *220*, 365.
(2) Martin, K. J.; Pinnavaia, T. J. *J. Am. Chem. Soc.* **1986**, *108*, 542.
(3) Carrado, K. A.; Kostapapas, A.; Suib, S. L. *Solid State Ionics* **1988**, *26*, 77.
(4) Giannelis, E. P.; Nocera, D. G.; Pinnavaia, T. J. *Inorg. Chem.* **1987**, *26*, 203.
(5) Park, I. Y.; Kuroda, K.; Kato, C. *J. Chem. Soc., Dalton Trans.* **1990**, 3071.
(6) Lal, M.; Howe, A. T. *J. Solid State Chem.* **1981**, *39*, 377.
(7) Dissado, L. A.; Hill, R. M. *J. Chem. Soc., Faraday Trans. 2* **1984**, *80*, 291.
(8) Giannelis, E. P. Gordon Research Conference, Zeolitic and Layered Materials, and personal communication, 1990.
(9) Brindley, G. W.; Kikkawa, S. *Clays Clay Mineral.* **1980**, *28*, 87.
(10) Miyata, S. *Clays Clay Mineral.* **1983**, *31*, 305.
(11) Schutz, A.; Biloen, P. *Solid State Chem.* **1987**, *68*, 360.
(12) Meyn, M.; Beneke, K.; Lagaly, G. *Inorg. Chem.* **1990**, *29*, 5201.
(13) Drezdzon, M. A. *Inorg. Chem.* **1988**, *27*, 4628.

0897-4756/92/2804-0922$03.00/0